Lab on a Chip

ROYAL SOCIETY OF CHEMISTRY

PAPER

View Article Online
View Journal | View Issue

Cite this: *Lab Chip*, 2025, **25**, 5538

Flip the chip: trapping a low number of cancer and immune cells for spheroid formation of homogeneous size

Raphael Dezauzier, Anna Fomina and Petra S. Dittrich *

Drug tests on patient-derived tumor cells enable a personalized therapy and promise early identification of resistant cells. However, most drug tests are performed on cell monolayers that do not resemble the complex tumor microenvironment. Spheroids are advanced models, as cells in 3D configuration exhibit cell–cell interaction, cell–extracellular matrix, and cell environment more similar to a tumor environment. In this study, we show the formation of homogeneous spheroids from a low number of cells, which is crucial for personalized drug tests with cells from tissue biopsies or liquid biopsies. We introduce a novel microfluidic platform that combines microwell technology with hydrodynamic trapping, thereby combining the advantages of both methods. The platform consists of trapping units, each comprising a microwell and a filter. Initially, the microwell is located on top, and the cells are homogeneously clustered by the filters. The chip is then flipped by 180°, allowing the cells to sediment at the bottom of the microwells, where they form spheroids protected from shear stress. We show that cells can be homogeneously captured along the array, while the filter geometry controls how many cells are captured per trapping unit. We explore several designs, each with different microwell and filter dimensions. With 91.5% capture efficiency, the cell loss is minimal. After turning the chip, spheroids of homogeneous size form in the wells and expand at a growth rate of 8 μm per day. We perform drug tests and show that cisplatin affects not only the viability of spheroids, but also their structural integrity. The drug ouabain octahydrate prevents the formation of spheroids by inhibiting cell–cell adhesion. Finally, we co-culture cancer cells and polarized macrophages. Macrophages can influence the susceptibility of tumors to drugs and indeed, we observe that spheroids co-cultured with M1-polarized macrophages have a lower viability after cisplatin treatment than spheroids without macrophages. In contrast, the presence of M2-polarized macrophages reduces the effect of cisplatin with more cells of the spheroids remaining viable. In summary, this platform has great potential for personalized drug tests, when a very low number of cells are available, for example cells derived from tissue biopsy samples, or circulating tumor cells obtained from liquid biopsies.

Received 28th February 2025,
Accepted 8th September 2025

DOI: 10.1039/d5lc00210a

rsc.li/loc

Introduction

Cancer is one of the deadliest diseases today, accounting for almost 10 million deaths and 18 million new cases worldwide every year.[1,2] A major issue when treating cancer patients is the diversity of cancer and the heterogeneity in tumors from patient to patient.[3–6] Moreover, the tumor profile of one patient can vary over time, due to mutations occurring in the composing cancer cells, and the development of resistance to treatment can occur. One way to solve this problem is to perform drug tests on cells originating from patient biopsies or liquid biopsies and to adapt and personalize the treatment.[7–10] However, standard methods perform these drug tests on microtiter plates, which lack control over the cell environment and require the use of large amounts of biological and chemical samples. Researchers have therefore developed microfluidic devices, which allow precise control of the environment of cells, while using very small liquid and biological quantities, due to the small size of the microchannels.[11,12]

While most drug tests are still performed with standard 2D cell monolayers, it recently has become clear that 3D models such as organoids and spheroids resemble more precisely the cell microenvironment.[13] Solid tumors are three-dimensional entities formed by tumor cells in a complex extracellular matrix (ECM). Cells in tumors exhibit different interactions between cells, between the cells and the ECM, and the cells and the environment than in 2D configurations,[13,14] which cause differences in drug response between 2D and 3D configuration.[15] Moreover, the tumor microenvironment (TME)

Department Biosystems Science and Engineering, ETH Zürich, Klingelberstrasse 26, Basel, 4056, Switzerland. E-mail: petra.dittrich@bsse.ethz.ch

is composed of cancer cells, immune cells, endothelial cells, and fibroblasts.[16] Immune cells such as macrophages play a significant role in tumor progression and metastasis. It is well-known that macrophages polarize into M1 and M2 phenotypes,[17,18] respectively, depending on the environment, *e.g.* the presence of certain signaling factors. M1-macrophages produce pro-inflammatory cytokines and reactive oxygen/nitrogen species, while M2-polarised macrophages can produce non-inflammatory cytokines, and promote angiogenesis and matrix remodeling. M1-macrophages are considered tumor-inhibiting, while M2-macrophages are tumor-promoting cells. When macrophages are integrated in the TME, referred to as tumor-associated macrophages (TAM), they may polarize in M1 and M2 macrophages, however, states beyond this dichotomy exist as well.[19] Besides the prognostic potential of TAMs, they can be also influenced by the drug treatment of the tumor and are also promising targets themselves for cancer therapy. The crucial role of macrophages in the tumor's fate under drug treatment makes it essential to implement them in the tumor models.

Standard methods to form spheroids from individual cells have been established, the most common one using non-adherent surface plates, ultra-low attachment well plates, and hydrogels. However, these techniques lack control over the size and environmental conditions of the spheroids, and they use large amounts of reagent and cells.[20,21] Microfluidic methods have addressed these bottlenecks.[22,23] For example, droplet microfluidic platforms have the advantage of creating homogeneous spheroids with high throughput,[24–27] but cells are exposed to a high shear stress inside the droplets, and the spheroids formed inside droplets are hard to access for following assays. Other versatile methods are the hanging droplet platforms, where cells are brought together using surface tension and gravity,[28,29] and microwells.[30–35] In most of these approaches, either the initial number of cells per compartment is not actively controlled and therefore can lead to non-homogeneous spheroid dimensions, or there is high cell loss. Alternatively, the use of traps to capture and cluster cells was introduced.[36–39] Here, the spheroids are always in contact with the flow inside the channel, required to keep them in position, therefore being constantly under the influence of shear stress, disrupting their viability and integrity. While the small dimensions of microfluidic devices are generally beneficial for further manipulation and analysis, most of these techniques require the use of a large quantity of cells to form spheroids and display a high amount of cell loss during formation. This is unproblematic when cancer cells from standard cultivation flasks are harvested, where the cell number is usually very high. However, the cell numbers of patient-derived cancer cells are usually very limited. Particularly, circulating tumor cells obtained from liquid biopsies are very rare cells. These cells are valuable sources for expansion and spheroid formation, where cell loss should be minimized as much as possible.

Here, we present a microfluidic strategy to produce spheroids from very few cells with minimal cell loss. The central part of the chip combines microwell technology with hydrodynamic cell trapping, combining the previously stated advantages of both methods. This was possible by the addition of a flipping mechanism, which makes the cell clustering and spheroid formation/culture independent from each other. The hydrodynamic trapping units ("filters") capture homogeneously virtually all supplied cancer cells, and allow to gain control over the number of cells that are trapped per microwell. Microwells are located above the trapping units. Simply by flipping the chip, captured cells are gently transferred into the wells by sedimentation. In the microwells, devoid of flow (and shear forces), the cells form spheroids, which can be monitored and subjected to drug tests. We employ this strategy to form homogeneous, small spheroids of the breast cancer cell line MCF-7, exploring various microwell and filter sizes. We then perform further drug tests (cisplatin and ouabain, a cardiac glycoside) on formed spheroids. To improve the model of solid tumors, we also co-capture immune cells (macrophages of different polarization), which were mixed with the breast cancer cells before injecting them in the chip.

Results and discussion

A. Chip design and functioning

The microfluidic chip is made of polydimethylsiloxane (PDMS), bonded to a glass slide. Cells are entering the chip through a serpentine channel (50 μm high and 300 μm wide) to increase the overall hydraulic resistance, making it more stable when the chip is flipped later or when the tubing is taken out of the system. The central part of the chip is an array of 20 traps, each trap consisting of two components: a filter and a microwell located on top of the trap (Fig. 1A and B). The filter has a gap of 6.5 μm, to trap efficiently cancer cells with a typical size of 12–25 μm.[40,41] The microwells located on top of the traps have a diameter of 200 μm, a filter arc length of 240 μm, and are 220 μm deep to carry the final spheroids. After MCF-7 cells are trapped, the chip is flipped by 180° and cells sediment into these wells (Fig. 1C). The chip is coated with a cell-repellent coating, which does not allow the cells to adhere to the surface of the well. After an overnight incubation, the cells naturally agglomerate into spheroids (Fig. 1D).

In a typical experiment, we inject *ca.* 600 cells into the chip. The cells are trapped at the filter (Fig. 2A) with a homogeneous distribution between the different traps. Each trap has a hydraulic resistance R given by the following equation:[42]

$$R = \frac{12\eta l}{wh^3} \quad (1)$$

where η is the viscosity of the fluid, l the length of the channel, w the width and h the height. Once cells start to fill a trap, the available width of the filter will decrease, the hydraulic resistance of this trap will increase (Fig. 2B), so that the flow rate through the trap will decrease. This allows self-regulating trapping, where cells will be homogeneously trapped all along the array. Simulation on a simplified model, shown in Fig. S1,

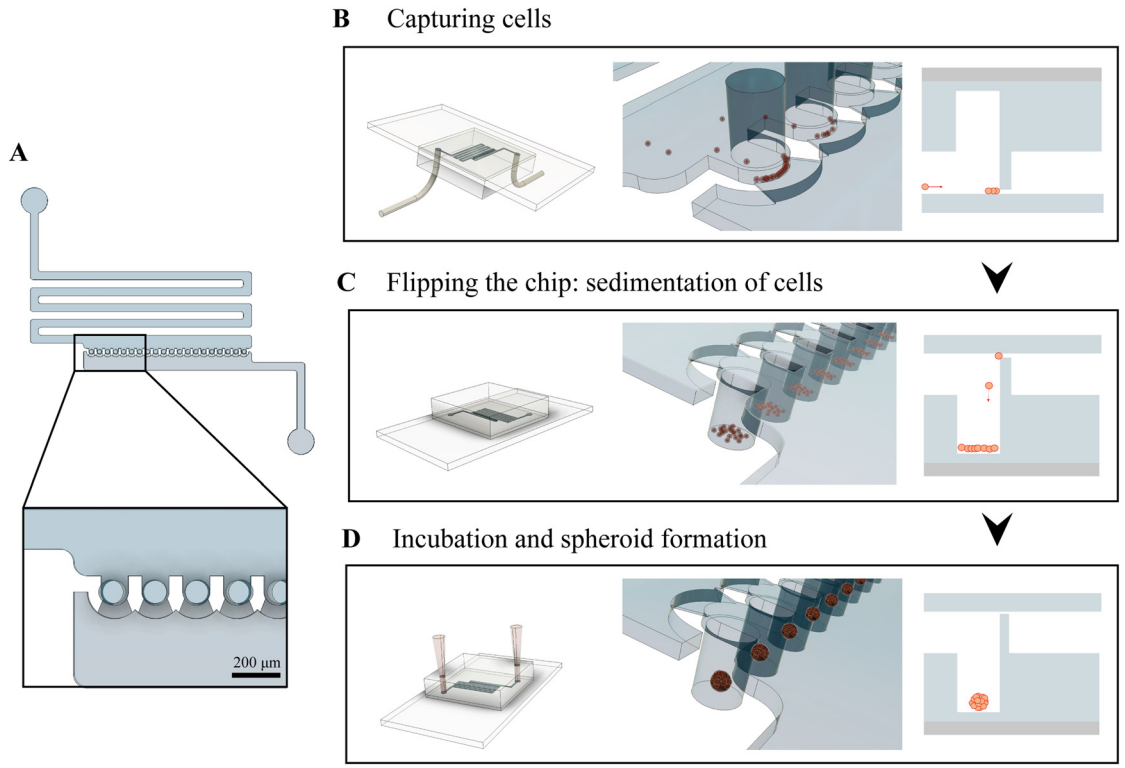

Fig. 1 "Flipping chip" working principle. (A) 3D rendering of the microfluidic device. The serpentine channel leads the cells to the trapping and culturing units. (B)–(D) Operation of the device. (B) Cells are injected *via* tubing and captured in the trapping unit. The side view (right) shows the moment when cells are trapped at the filter. The small gap of 6.5 µm allows medium and small debris to pass, but the larger tumor cells are physically trapped. In this initial process, the microwells are located on top of the filter. (C) After cell supply, the chip is flipped, and the cells sediment into the microwells which are now under the filter. (D) The chip is placed in an incubator. Due to a non-adherent coating in the microwells, the cells aggregate together and form spheroids overnight.

illustrates this principle. When counting the number of escaped cells as compared to the number of trapped cells, we observe a trapping efficiency of 91 (±5) % (Fig. 2D). We define trapping efficiency as the number of cells captured by the filter, *versus* the number of cells counted in the outlet tube. Cell loss might however occur in the tubing, due to adhesion or settling of cells. We enumerate the total number of cells required to fill all twenty traps to form spheroids (Fig. 2E). After capturing, the chip is flipped by 180° and the cells located on the filter naturally sediment inside the microwells which are now located under the trap. Only between 400 and 800 cells are required to form 20 spheroids in our device. To underline the effect of the filter, we also filled the microwells without using the filter, *i.e.* the cells are injected when the microwells are at the bottom. In this case, the cells fill the microwells but are not trapped in the filter and hence, there is no change of the resistance. We calculated the probability density function over four different chips for both condition (Fig. 2F). We find that the use of the filters improves the homogeneous distribution of cells. Without filters, some microwells are overfilled while others remain hardly filled. Although we obtain similar values for the mean (32.6 cells with filters and 32.3 cells without), the use of the filters provides a much lower standard deviation and coefficient of variation (SD of 8.2, CV of 25.6%) than without (SD of 20.5, CV of 62.9%).

We explored further geometries. The "Large Well Design" (LWD) (Fig. 2G) uses the same working principle, but has 10 microwells of 500 µm in width, and a filter arc length 572 µm. The larger filter allows the capturing of 71.2 (±18.7) cells (Fig. 2G), more than twice the number of cells caught by the "Small Well Design" (SWD) used above. The "Two-Filter Design" (TFD) has 10 large 500 µm wells but displays two different filter length (173 and 572 µm), alternating between wells (Fig. 2H). When trapping cells using the TFD, we observe the trapping of 52.5 cells in wells with small filters, and of 103.6 cells in wells with large filters. In conclusion, the filters facilitate not only homogeneous trapping of cells but provides also control over the number of cells that are trapped per microwell.

B. Simulation of shear stress

It is of crucial importance that cells remain viable after the initial clustering process. Shear stress is one of the most important physical effects that could be detrimental to cell viability.[43,44] For example, it was reported that the viability of circulating breast cancer cells was reduced above a wall shear stress of 5 dyn cm^{-2}.[45] The microfluidic chip was therefore designed in a way to limit the shear stress on cells while keeping an efficient trapping and spheroid formation. The

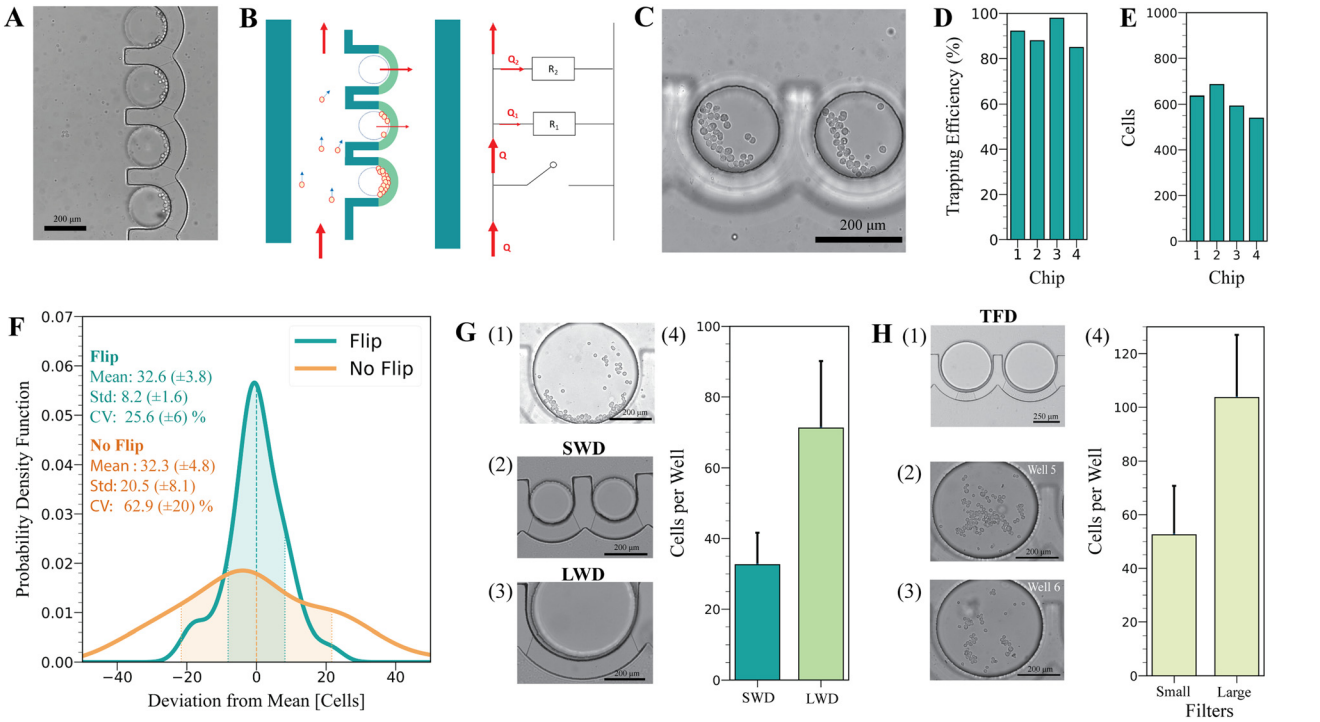

Fig. 2 Cell trapping and clustering. (A) Microscopy image of MCF-7 cells that are trapped in the filter. (B) Schematic of the hydrodynamic principle used to cluster the cells homogeneously. Each trap has a hydraulic resistance. Once a trap is filled with cells, its hydraulic resistance increases, and next cells will be more prone to fill other traps. (C) Microscopy images of the captured MCF-7 cells in the microwells, after flipping the chip. (D) Trapping efficiency in 4 different chips (N = 4). The efficiency is calculated by dividing the number of trapped cells by the sum of escaped cells and trapped cells. (E) Total number of cells captured per chip, in four different chips (N = 4). (F) Probability density function of cells per microwell (N = 4, n = 80), when filters are used for trapping and the chip is flipped afterwards, or when the filters are not used (microwells are already at the bottom during cell injection and the chip is not flipped). Statistical values from N = 4 chips per condition. (G) Test of two different well sizes; (1) microscopy images of cells trapped by large filter. (2) Image of the "Small Well Design" (SWD). (3) Image of the "Large Well Design" (LWD). (4) Number of cells clustered per microwell (LWD: N = 4, n = 40; SWD: N = 4, n = 80). (H) Test of two different filter designs; (1) microscopy images of large and small filters in the "Two Filter Design" (TFD) (2) cells trapped by large filters. (3) Cells trapped by small filters. (4) Number of cells clustered per microwell, for small filter and large filter in TFD (N = 2, n = 10 per condition).

shear stress inside the traps is highest at the filter's border (between 1.5 and 4.9 dyn cm^{-2}), where the fluid is most constrained, and the velocity gradient increases (SWD, Fig. 3A). The shear stress is reduced drastically in the other areas of the traps, where the cells experience a shear stress below 0.5 dyn cm^{-2}. These values do not exceed critical shear

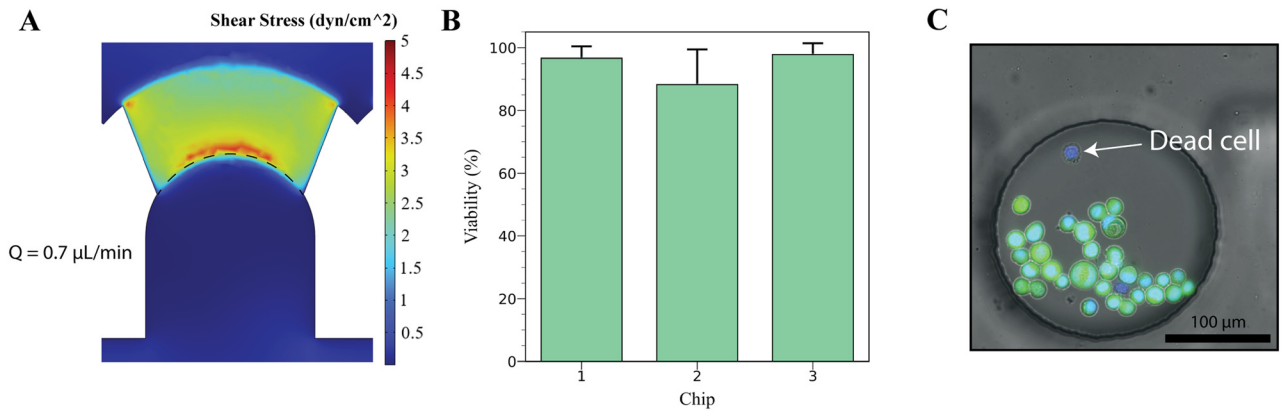

Fig. 3 Viability of MCF-7 cells after capturing. (A) Simulation of the shear stress inside the microfluidic chip during the trapping. The flow rate in the chip is set to 0.7 µL min^{-1}. The black dashed line indicates the position of the filter. (B) Viability measurement after clustering of three different chip replicates (N = 3, n = 60). (C) Microscopy images of the viability testing right after the clustering step. Calcein AM (green) was used to stain live cells, while NucBlue (blue) was used to stain all cells. The arrow indicates a dead cell without intracellular green fluorescence.

stress levels for mammalian cells.[8] Live/dead assay performed on cells after clustering confirm a high viability of 94 (±8.16) % (Fig. 3B and C).

C. Spheroid formation

Once spheroids are formed, we use hydrostatic pressure realized by two pipette tips at the inlet and outlet for supplying fresh media. As spheroids are already settled in the microwells they do not experience a flow disturbance during this procedure. We compare the formation of spheroids inside the SWD, and in the LWD (Fig. 4A). We observe a diameter of 70.5 (±7.2) μm for SWD, and a diameter of 95.0 (±9.83) μm for LWD, 48 h after cell clustering (Fig. 4B). As more cells in the LWD are trapped, the spheroids are larger. In both designs the sizes are homogeneous, with a CV of 10.5% for SWD and of 9.7% for LWD (Fig. 4C).

We also use the circularity C as a means to characterize the spheroids, determined by the following equation:

$$C = \frac{4\pi A}{P^2} \quad (2)$$

where A is the area of the spheroid, and P is the perimeter. A circularity of 85.3 (5.93) % for small wells and 82.7 (9.5) % for large wells is observed (Fig. 4D), suggesting that the spheroids are healthy in both designs, while spheroids with disaggregating cells or with low attachment between cells would display low circularity.[33] It should be noted that in both designs only a single spheroid is formed (97.5% for SWD, and 92.3% for LWD, Fig. 4D), which is crucial for later drug tests and reproducibility. Sometimes, it can be observed that one of few cells are not attached to the main spheroid, probably being non-viable cells (6% of cells are non-viable after clustering).

In the following part of this study, we always use the small well design. Fig. 4F shows a spheroid with stained F-actin cytoskeleton and nucleus retrieved after 5 days of culture. The spheroids are located in a controlled environment in the wells, protected from flow perturbations (Fig. 4G). A flow rate of 2 μL min^{-1}, slightly higher than the flow rate during media exchange (Fig. S3C), would result in shear stress on the spheroid lower than 0.01 dyn cm^{-2}, which is completely negligible. The geometries also allow for the use of higher flow rates, as can be seen in Fig. S3D. This allows to cultivate the spheroids in stable conditions for at least 11 days after trapping, with the spheroids displaying a constant average growth rate of 8 μm per day (Fig. 4H).

D. Drug test on spheroids using cisplatin

Next, we proceeded with a drug test on spheroids, using the well-known anti-cancer drug cisplatin. Cisplatin molecules

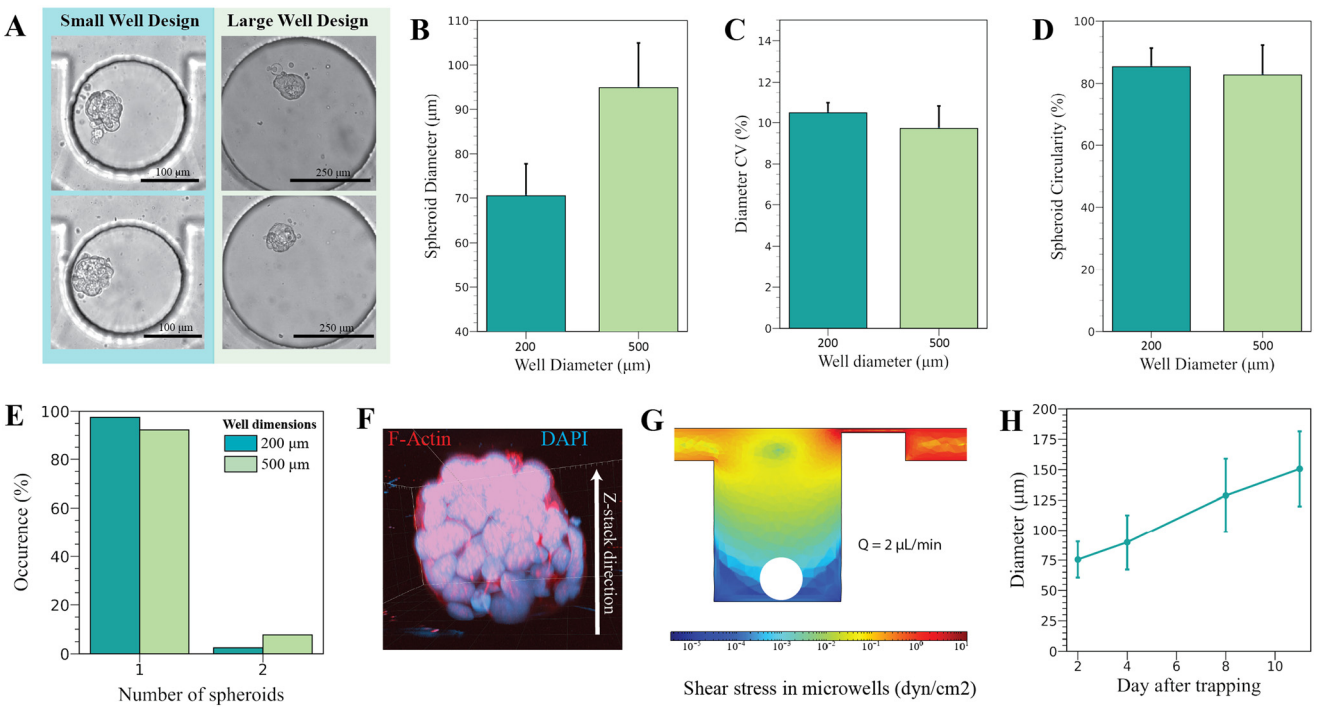

Fig. 4 Spheroid formation. (A) Microscopy images of the MCF-7 spheroids 48 h after clustering, for the "Large Well design" and the "Small Well design". (B) Diameter of spheroids, 48 h after the clustering step for both designs (LWD: N = 4, n = 39; SWD: N = 4, n = 80). (C) Coefficient of variation (CV) of spheroid diameter across four chips per conditions (N = 4). (D) Circularity of spheroids for both designs (LWD: N = 4, n = 39; SWD: N = 4, n = 80). (E) Distribution of the number of spheroids per well (LWD: N = 4, n = 39; SWD: N = 4, n = 80). (F) Confocal microscopy stack of a spheroid retrieved a week after clustering. Phalloidin was used to stain the F-actin cytoskeleton (red), and NucBlue™ was used to stain the nucleus (blue). (G) Simulation of the shear stress inside the microwells for SWD, for a flow rate of 2 μL min^{-1}. The white circle inside the microwell represents the space a spheroid would occupy 48 h after clustering. (H) Growth curve of the spheroids inside the microwells for SWD (N = 2, n = 40).

interfere with DNA replication, therefore targeting cells with high proliferating capacities, such as cancer cells.[46] The spheroids, which were prior cultured for 6 days after cell clustering, were exposed to different concentrations (0, 50, 100, 200 μM) of cisplatin and incubated for 12 hours. After this time, the media concentrated with drugs was washed away, and the spheroids were cultured up to four more days. Viability tests over time (2,3 and 4 days after cisplatin incubation) were conducted with live/dead cell assay. We use a viability score defined by the ratio of the volume of live (green) to dead (red) cells that we obtained from the fluorescence images (Fig. 5A). Initially, the viability score of the spheroids was >94%, but dropped with increasing drug concentrations (Fig. 5B). Non-treated spheroids maintained a high viability score over the four days. Between day 3 and day 4, it seems the drug has no more effect on the spheroids, and a slight increase in viability for 50 μM and 200 μM can be explained by the degradation of dead cells which are no longer fluorescent. Cisplatin also affects the integrity of the spheroids, as cells detach from them, therefore increasing the perimeter, and decreasing the circularity (Fig. 5C). For a concentration of 200 μM, no spheroids can be observed anymore after only two days, just a random agglomeration of cells. 3 days after cisplatin incubation, the IC50 is determined to be 75.69 μM (Fig. 5D). These results are consistent with prior studies, where spheroids are cultured in microwells.[33] To confirm the removal of drug, we additionally characterized the washing efficiency using sulforhodamine B (SRB) (Fig. 5E). After the first hydrostatic wash, the concentration of SRB is diluted from 10 μM to 0.018 μM, or 556×. After the second wash, the concentration is 0.0027 μM, or a dilution of 3703×.

E. Effect of ouabain on the formation of breast cancer cell spheroids

Next, we study the effect of another drug on the formation of the spheroids. Ouabain octahydrate is a cardiac glycoside, used

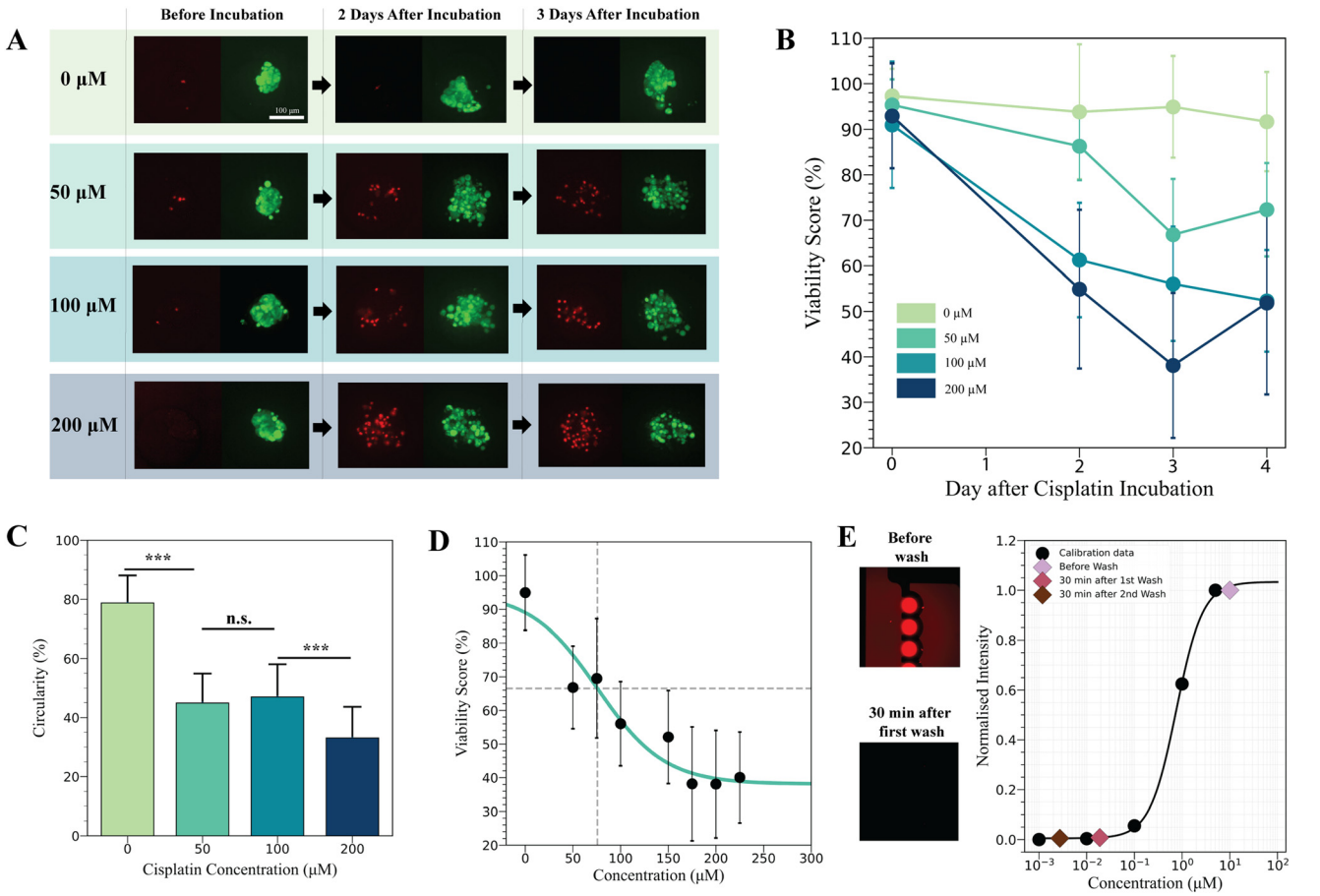

Fig. 5 Drug test on MCF-7 spheroids with cisplatin. (A) Fluorescence images of the spheroids for different cisplatin concentrations and times. Fluorescence images are the projections of the sum of the stack intensities. Calcein AM was used to stain live cells. Draq7 was used to stain dead cells. (B) Effect of cisplatin incubation on spheroid viability over time. For $c = 0$ μM: $N = 1$ and $n = 16$. For $c > 0$ μM: $N = 2$ and $n > 32$. (C) Circularity of the spheroids 3 days after incubation ($N = 2$, $n > 39$ for each concentration, control: $N = 1$, $n = 18$). (D) Viability score measurement after 3 days, for several concentrations, with fitted IC50 curve. For $c = 0$, 75, 225 μM: $N = 1$ and $n > 15$. For other c: $N = 2$ and $n > 36$. (E) Washing procedure in the device. Left: Microscopy images of wells with 10 μM sulforhodamine B (SRB), and after 30 minute hydrostatic wash. Right: Calibration curve, established by measuring intensity in microwells for different SRB concentrations. Colored symbols represent measurements before and after washing steps.

to treat hypotension and arrhythmias. Although this compound has been studied extensively in the case of heart disease, recent studies suggest that this drug could have a cytotoxic effect on cancer cells.[47,48] Moreover, Gkountela *et al.* have shown that ouabain octahydrate could be used to prevent metastasis formation, by inhibiting cell–cell junction formation in circulating tumor cell clusters and reducing the size of cell clusters. As ouabain inhibits Na/K-ATPase, it can inhibit cell–cell junction formation through the increase of intracellular Ca^{2+} concentration.[49] Based on these previous findings, we here hypothesize that ouabain influences or even prevents the formation of spheroids, even at concentrations where cell viability is not affected. First, we assessed the viability of the cells for different concentrations of ouabain on- and off-chip (Fig. S6). Both cells in flask and spheroids in chips remained viable for a concentration of 20 nM, in accordance with a previous study.[49] Next, the cells were pre-cultured in flasks and then clustered inside the chips, where they are incubated with or without ouabain (Fig. 6A and B). Circularity measurements were used to estimate the spheroids shape (Fig. 6C). We observe a significant loss of circularity when the cells are cultured with the drug (13% drop, $p = 1.4 \times 10^{-5}$) and an additional significant loss of circularity when the drug treatment continued on-chip (13% drop, $p = 1.5 \times 10^{-5}$). In both cases, fewer cells form the spheroid-like assembly, while many remain isolated. Moreover, the spheroids display fewer round shapes, suggesting less adhesions between the cells. In contrast, no loss of circularity was observed when cells were cultured without the drug in the flask, but with added drug during spheroid formation. These results demonstrate that the effect on the spheroid formation requires prior incubation with ouabain and is not an immediate effect. At this concentration, ouabain may thus prevent cluster formation of CTCs, but not the integrity of already formed solid tumors.

F. Formation of heterogeneous spheroids

Finally, we demonstrate the possibility of performing co-cultures inside our chip. We trap M0 macrophages, differentiated from THP-1 monocyte, together with MCF-7 cancer cells by injecting a cell suspension with a 1 : 5 ratio of both cell types. In parallel, we use a second, more aggressive breast cancer cell line, MDA-MB-231 and trap them with MCF-7 cells, using a cell suspension with 4 : 5 ratio. Example of the spheroids for both co-cultures can be seen in Fig. 7A. In the case of macrophages with MCF-7 co-culture, we observe the full or partial integration of the cells into the MCF-7 spheroid (Fig. 7B). In contrast, MDA-MB-231 form their own spheroid separated from the MCF-7 spheroid. In most cases, the two spheroids are attached to each other, but a clear distinction between the cell lines can be observed. This is further confirmed by the circularity measurement (Fig. 7C). M0/MCF-7 spheroids have a slightly lower circularity than pure MCF-7

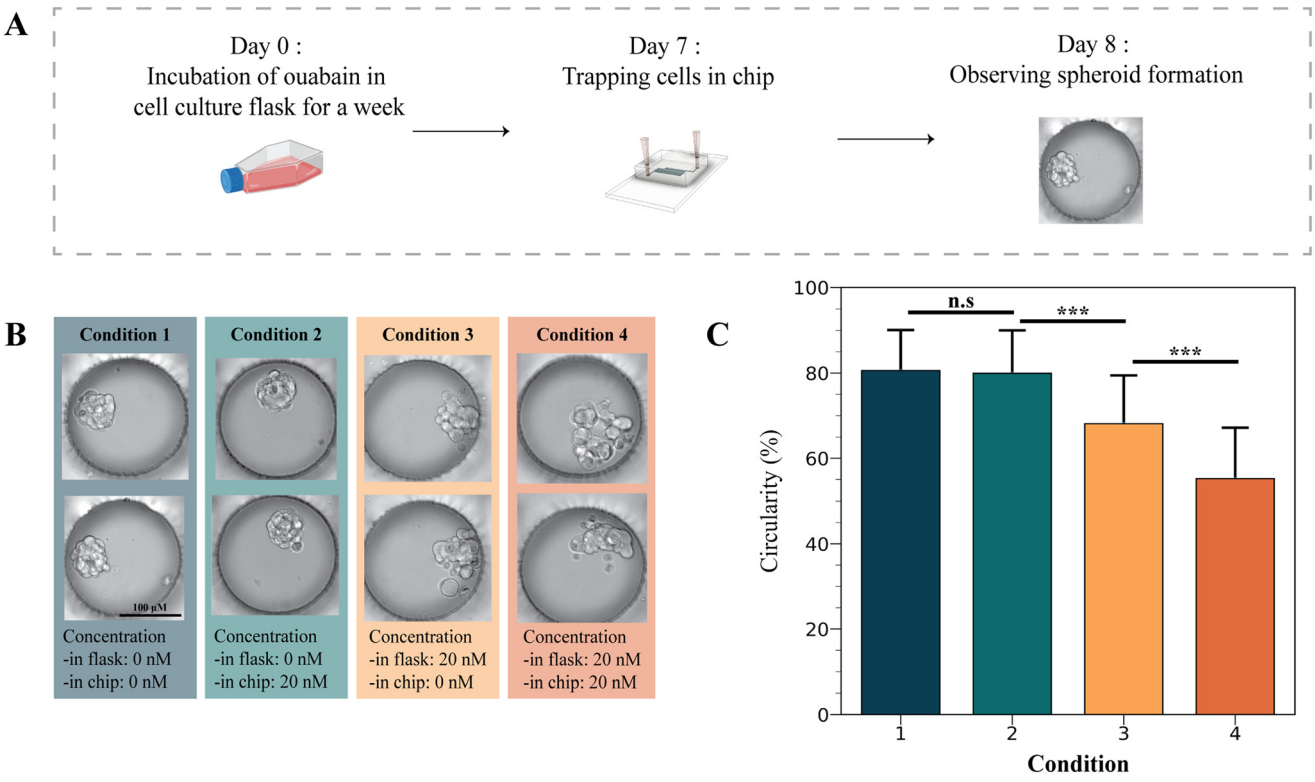

Fig. 6 Testing the effect of ouabain octahydrate on spheroid formation. (A) MCF-7 cells are incubated inside the cell culture flask with ouabain for 1 week. Then, spheroids are formed on-chip. The shape of the spheroids is studied on day 8. (B) Example micrographs of spheroids formed under different conditions as indicated in the figure. (C) Circularity of the spheroids depending on the conditions of ouabain incubation ($N = 2$, $n > 37$ for each condition).

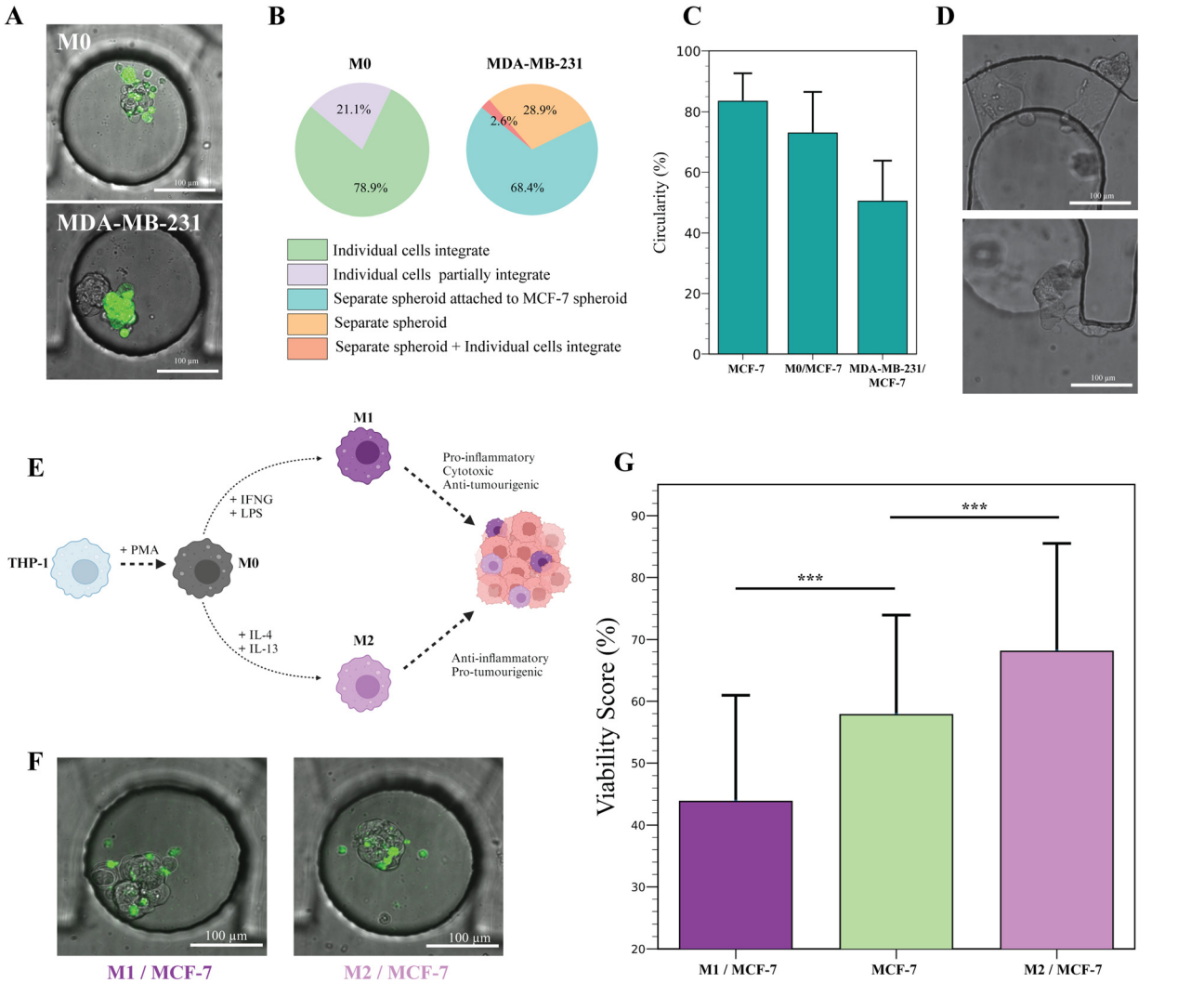

Fig. 7 Co-culture with polarized macrophages and different cancer cells. (A) (top) Spheroids formed in the presence of M0 macrophages (M0/MCF-7 spheroids) and (bottom) MDA-MB-231 (MDA/MCF-7 spheroids). M0 and MDA-MB-231 cells are stained using CellTracker™ Green CMFDA Dye before trapping. The stains last for at least 48 h. (B) Behavior of other cell types (M0 macrophages and MDA-MB-231) when co-cultured with MCF-7. N = 2 and n = 38 for each condition. (C) Circularity of M0/MCF-7, MDA/MCF-7, and MCF-7 spheroids 48 h after clustering. N = 5 and $n >$ 85 for co-culture conditions, and N = 3, n = 60 for control MCF-7 spheroids. (D) Migration of MDA/MCF-7 spheroids out of well on day 8 of culture. (E) THP-1 monocytes can be differentiated into M0 adherent tumor-associated macrophages. By adding IFNG and LPS, they polarize into M1 macrophages, which have anti-tumorigenic properties. By adding IL-4 and IL-13, M0 macrophages polarize into the M2 phenotype, which have pro-tumorigenic properties. (F) Spheroids formed in presence of M1 polarized macrophages (left) and M2 polarized macrophages (right), 48 h after clustering. M1 and M2 cells are stained using CellTracker™ Green CMFDA Dye before trapping. (G) Viability score of spheroids after 100 µM cisplatin treatment (N = 5, n = 90 for M1/MCF-7, N = 4, n = 71 for M2/MCF-7, N = 5, n = 86 for MCF-7). The viability scores are all normalized on the mean value of each control experiment.

spheroids, due to the presence of some individual, not integrated cells around the spheroid. MDA/MCF-7 co-culture has much lower circularity as both spheroids together are used for the determination of circularity. We assume that the difficulty in forming MDA/MCF-7 spheroids is originated by the different expression of E-cadherin in both cell lines. E-cadherin is the major protein mediating cell–cell adhesion in MCF-7 spheroids,[50,51] however, MDA-MB-231 do not express this protein.[52] We cultured the heterogeneous spheroids over several days and observed similar growth of the M0/MCF-7 spheroids compared to pure MCF-7 spheroids (Fig. S7). However, it is worth noting that in M0/MCF-7 spheroids, MCF-7 will outgrow the non-proliferating M0 monocytes. Interestingly after some days of culture, for MDA/MCF-7 spheroids, we often observe the migration of the spheroids out of the microwell (Fig. 7D). The MDA spheroid attaches to the walls, then escapes from the microwell together with the MCF-7 spheroid. Even more surprisingly, we can observe in some cases that the migration of spheroids appears on the side of the filter, where the cells deform, pass through the 6.5 µm gap and escape. At this point, we have refrained from further systematic investigation of this unexpected behavior of increased mobility and plasticity, which is the focus of future work, and continued with the macrophage/MCF-7 spheroids.

Next, unpolarized macrophages (M0) are polarized into M1 and M2 macrophages by treatment with INF-γ/LPS and the interleukins 4 and 13 (IL-4, IL-13), respectively (Fig. 7E) according to our previous protocols and characterizations.[53] Polarized macrophages and MCF-7 cells are co-injected and form heterogeneous spheroids (Fig. 7F). The spheroids are cultured for a week, before being exposed to a 100 μM cisplatin solution for 12 h. Spheroids composed of only MCF-7 cells are also cultured for comparison. Following cisplatin administration, we noticed a significant difference between the viability of M1/MCF-7 and M2/MCF-7 spheroids (Fig. 7G). M1/MCF-7 spheroids exhibited a viability score of 44%, while M2/MCF-7 spheroids had a viability of 68%, therefore a significant difference between the two conditions of 24% ($p = 3.4 \times 10^{-14}$). Also, both conditions exhibit significant differences in viability with MCF-7 only spheroids, which display a viability score of 58%. These results could be explained by the pro and anti-tumorigenic nature of M1 and M2 macrophages. M1 macrophages secrete TNF-α, a cytokine activating apoptosis pathways in cancer cells.[54,55] Moreover, they produce reactive oxide species (ROS), including superoxide anions, hydrogen peroxides and nitric oxide (NO), which damage cellular components and prevent DNA repair pathways.[56] Cisplatin targets DNA replication and transcription by forming DNA crosslinks,[46] and the apoptosis process might be promoted by previous DNA damage and lack of repair mechanism provoked by ROS. It also has been shown that cisplatin induces an increase in TNF-α and NO in macrophages, therefore increasing their effect on cancer cells.[57,58] On the other hand, M2 macrophages stimulate cancer cell proliferation *via* epidermal growth factor (EGF) and can protect them from chemotherapy toxic effect by secreting survival factors (IL-6 or osteopontin).[59] Furthermore, there is evidence that exosomes produced by M2-macrophages are involved in cisplatin resistance from cancer cells. These exosomes would transport microRNA-21, which suppresses apoptosis and enhances activation of the PI3K/AKT signaling pathway, provoking tumor progression.[58,60] While the effect of secretions from M1 and M2 macrophages on cancer cells are documented in literature, we here did not include measurement of cytokine, exosomes or ROS secretion, which is the focus of future work. Moreover, in DMEM media, it is possible that the macrophages lose their polarization over time. Therefore, the effect of macrophages could diminish over time. Nevertheless, our results demonstrate the importance of considering the heterogeneous nature of tumors. Our platform allows us to form an improved model of the tumor in a facile way and to study the interactions of cancer and immune cells under treatment with chemotherapeutic drugs.

Conclusion

We have introduced a microfluidic method to trap cancer cells for subsequent spheroid formation from minimal cell number. The design of the device with filter structures and culture wells, combined with a flipping mechanism, allows to uncouple deterministic cell capture from culture and spheroid formation under gentle conditions without shear stress. We have demonstrated that the filter structures capture cells homogeneously across the array and give control over the number of cells that can be captured per well. Subsequently, viable spheroids of homogeneous size and circularity can be reliably formed in different sizes of microwells. Moreover, heterogeneous spheroids consisting of cancer cells and unpolarized or polarized macrophages were successfully formed. Subsequent drug tests with the conventional cancer drug cisplatin underlined the relevance of advanced cancer models, as the immune cells influence the viability of the cancer cells under drug exposure. The microfluidic method can be further employed to investigate effects on spheroid formation and prevention of cell clustering as demonstrated with the tests using the drug ouabain. Notably, we needed only a low number of cells for the spheroid formation, as almost all injected cells are captured, although cell loss occurs in the tubing, which may need some attention and improvement in future device designs. The few injected cells distributed evenly across the trapping units. We therefore anticipate that our device could be used in clinical settings, with patient sample from tissue biopsies. Moreover, circulating tumor cells in blood or other body fluids such as ascites are usually very rare cells and we believe that our device opens a possibility to culture the few filtered cells in a more efficient way than previous studies showed,[8] particularly because our new method protects the sensitive CTCs from continuous shear stress. For other applications, the number of wells could be increased for a higher throughput and the channels could be parallelized to create more experimental conditions, *e.g.* enabling comparable, standardized drug tests on a single platform.

Experimental

Microfluidic design and simulation

The chip was designed with 2D CAD software AutoCad (version 2025, Autodesk), used to print the foil photomasks for mold fabrication (Selba S.A). To perform simulations, the chip was also modelled in 3 dimensions using Fusion 360 (AutoDesk). The model could be imported in the finite element model software Comsol Multiphysics® 6.0. The laminar flow module was used with a stationary study. The inlet, outlet, and flow rate were defined to obtain the shear rate. By multiplying the value of shear rate with the viscosity of the liquid, we could therefore estimate the shear stress all along the chip for different flow rates. To show the maximal shear stress inside the trap during capturing, we put the plane at 0 μm.

Chip microfabrication

The silicon/SU-8 master mold was fabricated using photolithography (Fig. S8). Three layers of the photoresist SU-8 are processed, corresponding to the three heights in the final mold. The first layer defined the gap of the filter, the second the height of the channel, and the third the depth of the wells. For the first layer, a thin 6.5 μm layer of SU-8 3005 (SU-8 3000 series, Kayaku) was deposited *via* spin coating onto a plasma-cleaned

silicon wafer. The height of the layer was determined by the velocity profile of the spin coater, which was chosen to be 6000 rpm with an acceleration/deceleration of 100 rpm. After a soft bake (T = 65 °C for 1 min, T = 95 °C for 2 min), the photoresist was exposed through the photomask with UV light, at an exposure intensity of 600 mJ cm^{-2}, inside a mask aligner (MABA8-Gen3, Karl Suss). After post-exposure bake (T = 65 °C for 1 min, T = 95 °C for 2 min), the filter gap layer was finished, and the wafer could directly be used to spin coat the second layer. Here, SU-8 3050 was used, spin coated at a speed of 3000 rpm to reach 50 μm, followed by a soft bake (T = 65 °C for 1 min, T = 95 °C for 15 min). The wafer was again exposed through a second foil mask, and post-baked for 1 min at 65 °C and 5 min at 95 °C. The procedure differed slightly for the third layer, used for the depth of the wells. To reach a height of 220 μm, a layer of SU-8 3050 was spin coated at 1000 rpm, and then soft-baked for 1 minute at 65 °C and 45 minutes at 95 °C. Another layer was then spin coated with the same rotating parameters, followed by another soft baking step. Finally, the wafer was exposed through a third photomask and post-exposure baked. Afterwards, the wafer was placed in a solution of Mr-Dev-600 (MicroResistTechnologies) for 15 minutes before being rinsed with isopropanol alcohol (IPA) and DI water. The wafer was then hard-baked at 200 °C for 2 hours, with a ramp of 1.6 °C min^{-1}. Finally, the wafer was silanized inside a desiccator using perfluorooctyl trichlorosilane (PFOTS) (Sigma Aldrich). The chip was made of two layers of PDMS bonded together to form microchannels, bonded on a glass slide for support (Fig. S9). A ratio of 1 : 9 between Sylgard™ 184 Silicone Elastomer Curing Agent and Sylgard™ 184 Silicone Elastomer Base (Dow) was used. The elastomer solution was poured over the prepared master molds and cured for 3 h at 80 °C. Holes were made only in the top layer, to form the inlet and outlet of the chip. Plasma (Plasma Cleaner PDC-32G, Harrick Plasma) was used to bond the two PDMS layers, and to bond the chip to the glass slide. Tape was used before plasma treatment to get rid of dirt particules, and after bonding to cover the chip. The chip was cured again at 80 °C for at least 12 h.

Cell culture

The MCF-7 breast cancer cell line (ATCC) was cultured in Dulbecco's modified eagle medium (DMEM) (Gibco), containing 10% fetal bovine serum (FBS) (Gibco) and 1% penicillin–streptomycin at 37 °C, 5% CO_2. Cells were detached using phosphate buffer saline without magnesium and calcium (PBS) (Gibco) to wash the cells, and trypsin/EDTA (ThermoFisher) to detach them when cells reached confluency. Additionally, a MDA-MB-231 cell line (ATCC) was cultured in the same way as the MCF-7 cell line. THP-1 monocytes (ATCC) were cultured in Roswell Park Memorial Institute (RPMI) 1640 medium with GlutaMAX (Gibco), 10% FBS, and penicillin–streptomycin, passaged by diluting the medium. To differentiate THP-1 into M0 macrophages, 100 ng mL^{-1} PMA was added to the media for 3 days. M0 macrophages could be detached using TrypLE Express (Gibco). M0 macrophages were polarized to M1 macrophages by replacing the media with serum-free DMEM with 1 μg mL^{-1} LPS (ThermoFischer) and 100 ng mL^{-1} interferon-γ for 24 hours. Exposure of M0 macrophages to 50 ng mL^{-1} IL-4 (ThermoFischer) and 50 ng mL^{-1} IL-13 (ThermoFischer) for 48 hours resulted in M2-polarized macrophages.

Cell capturing and spheroid formation

The microfluidic chip was exposed to UV light for 10 minutes to activate the surface and prevent contamination. The microchannels were then coated using the cell-repellent surface coating anti-adherence rinsing solution (StemCell Technologies). To make sure that the coating was present also in the microwells, the chip was centrifuged at 400 RCF for at least 10 min. The syringe and tubing used for cell injection were also coated with the cell-repellent surface coating anti-adherence rinsing solution (StemCell Technologies). The chips were coated for at least 4 hours, before being washed with cell media. A cell suspension of 500 000–800 000 cells per mL was prepared. For co-cultures, cells are mixed in the cell suspension to the desired ratio and are all injected at the same time in the chip. To inject the cells inside the chip, poly(1,1,2,2-tetrafluoroethylene) (PTFE) tubing (BGB) were used, as well as Luer Locks adapters made of polyether ether ketone (PEEK, VWR). A syringe pump (Nemesys, Cetoni) was used to control the flow rates. The tubing was inserted inside the cell solution, and aspirated at a flow rate of 2.5 μL min^{-1}. Then the tubing was inserted in the device, and the chip was flipped by 180°. A flow rate of 0.7 μL min^{-1} was used for the small well design, and of 2.5 μL min^{-1} for the large well design and two filter design, for 1–5 min, until all traps were filled. Variation in time of injection is explained by the variability in time for cells to come out of the tubing. After capturing, the chip was flipped by 180°, and the cells sedimented at the bottom of the microwells. Pipette tips, filled with 200 μL media, were inserted inside the inlet/outlet. Chips were then placed in the incubator at 37 °C and 5% CO_2. To retrieve spheroids, the chip was flipped again, and a back flow was introduced to push out the spheroids. For chips used to measure capture efficiency, a backward flow rate was used post-flip to retrieve cells from outlet tube. Cells from the outlet and captured cells were counted to calculate the capture efficiency. This approach does not however take into account cell loss in the tubing.

Drug tests and washing procedure

For drug tests, a solution of cisplatin (Sigma Aldrich) was prepared. The powder was dissolved in PBS at 37 °C under constant mixing, to reach a concentration of 3.3 mM. The solution was stored at −20 °C. Additionally, a solution of ouabain (Sigma Aldrich) was prepared. The powder was dissolved in ultra-pure water at 37 °C under constant mixing to reach a concentration of 20 mM. The solution was also stored at −20 °C.

Spheroids were cultivated for 6 days and then treated with the drugs if not specified otherwise. The drug was supplied and incubated for 12 hours. Then the drug is washed out by

addition of drug-free medium, followed by an incubation for 30 minutes. This procedure is repeated a second time.

We characterized the washing efficiency using sulforhodamine B (SRB). A calibration curve was determined by injecting an aqueous SRB solution at concentrations between 0.001 to 10 μM. Subsequently, 10 μM SRB was supplied and the washing procedure above was conducted. Dilution factors could be determined from the calibration curve.

Imaging

To calculate the viability of spheroids, the spheroids inside the chip were imaged in three dimensions by confocal microscopy. Media containing 1 μM of calcein AM (green fluorescent) (Thermo Fischer) and 10 μM DRAQ7 (red fluorescent) (Thermo Fischer) was supplied, and the chip was incubated at 37 °C and 5% CO_2 for 45 minutes. The spheroids were then washed, and the chip were placed on the confocal microscope (custom-made fluorescence microscope with spinning disk unit from Visitron). For each spheroid, a stack of 21 images was taken, with a distance of 5 μm between each image. Stack images were then analyzed to obtain a viability score (see section Spheroid and cell analysis). To image retrieved spheroids, Phalloidin eFluor™ 660 (ThermoFischer) was used to stain the F-actin cytoskeleton, while NucBlue™ (ThermoFischer) was used to stain nuclei. The spheroids were placed on a thin glass slide and imaged with a stack resolution of 1 μm using the LSM 980 (Zeiss) confocal microscope. Imaris 10.2 software was used to visualize the stack in 3 dimensions. Viability measurements of cells after trapping were performed using Nikon Eclipse Ti2. NucBlue™ was used to stain all cells, whereas calcein AM was used to stain live cells. Brightfield images were taken using either Nikon Eclipse Ti2, Olympus IX71, or a Visitron custom-made microscope.

Spheroid and cell analysis

The circularity, diameter of the spheroids, and number of cells captured per well were extracted using ImageJ from brightfield images. The viability was derived by means of a home-made Python software (Fig. S10). The software allows importing the stack images and classifying the images by experimental parameters (time, chip ID, drug concentration). A Boolean mask is created for each slice of the stack, using the Otsu thresholding method.[61] The number of pixels above the threshold is counted, and the positions of the pixels in the images are also registered. When all the slices have been analyzed, the sum of the different areas gives the total "volume" of fluorescence for the stacks. This procedure is done for the green and red fluorescence detection channel, corresponding to live and dead stained cells. The ratio between the "volume" of live cells and dead cells gives the viability score. As Draq7 stains the nucleus and Calcein AM stains the cytoplasm, the dead "volume" is increased by a size factor of 4.62 (cytoplasm radius^3/nucleus radius^3 = $20^3/12^3$).

Data analysis and figure creation

Data was stored in Excel files. They were analyzed and displayed in graphs using Python Jupyter Notebook. A Mann–Whitney U statistical test is used to calculate the *p*-value used to determine the significance of the difference between certain measurements ($p < 0.05$: *, $p < 0.01$: **, $p < 0.001$: ***). The figures were created using Adobe Illustrator. Some sketches (Fig. 6A and 7E) were created with **https://www.BioRender.com**.

Author contributions

R. D. designed and fabricated the device, performed experiments, made simulations, programmed the analysis software, and evaluated the data. A. F. performed co-culture experiments and evaluated the data. P. S. D. conceptualized and supervised the work. R. D. and P. S. D. wrote the manuscript.

Conflicts of interest

There are no conflicts to declare.

Data availability

Supplementary information is available, and contains further explanations concerning device fabrication, working principle, simulations, experiments and image analysis. See DOI: **https://doi.org/10.1039/D5LC00210A**.

The data for the study is available at Zenodo. This includes exemplary images for every figure and graph; the excel files with data for the graphs including the code for analysing the data; simulations. Link: **https://zenodo.org/records/14884609**.

Acknowledgements

We thank S. Svanberg and L. Stöcklin for their support with cell culture. We thank the D-BSSE Clean Room Facility and the D-BSSE Single Cell Facility for access and support. The study is supported by the strategic focus area of Personalized Health and Related Technologies at ETH Zurich (PHRT-541).

Notes and references

1 J. Ferlay, M. Colombet, I. Soerjomataram, D. M. Parkin, M. Piñeros, A. Znaor and F. Bray, *Int. J. Cancer*, 2021, **149**, 778–789.
2 H. Sung, J. Ferlay, R. L. Siegel, M. Laversanne, I. Soerjomataram, A. Jemal and F. Bray, *Ca-Cancer J. Clin.*, 2021, **71**, 209–249.
3 R. Fisher, L. Pusztai and C. Swanton, *Br. J. Cancer*, 2013, **108**, 479–485.
4 A. Skibinski and C. Kuperwasser, *Oncogene*, 2015, **34**, 5309–5316.
5 I. Dagogo-Jack and A. T. Shaw, *Nat. Rev. Clin. Oncol.*, 2018, **15**, 81–94.
6 A. Marusyk and K. Polyak, *Biochim. Biophys. Acta, Rev. Cancer*, 2010, **1805**, 105–117.

7 B. L. Khoo, G. Grenci, T. Jing, Y. Bena Lim, S. C. Lee, J. P. Thiery, J. Han and C. T. Lim, *Sci. Adv.*, 2016, **2**, 1600274.
8 F. D. Schwab, M. C. Scheidmann, L. L. Ozimski, A. Kling, L. Armbrecht, T. Ryser, I. Krol, K. Strittmatter, B. D. Nguyen-Sträuli, F. Jacob, A. Fedier, V. Heinzelmann-Schwarz, A. Wicki, P. S. Dittrich and N. Aceto, *Microsyst. Nanoeng.*, 2022, **8**, 130.
9 G. C. Napoli, W. D. Figg and C. H. Chau, *Front. Med.*, 2022, **9**, 912641.
10 J. Zhai, C. Li, H. Li, S. Yi, N. Yang, K. Miao, C. Deng, Y. Jia, P. I. Mak and R. P. Martins, *Lab Chip*, 2021, **21**, 4749–4759.
11 S. Halldorsson, E. Lucumi, R. Gómez-Sjöberg and R. M. T. Fleming, *Biosens. Bioelectron.*, 2015, **63**, 218–231.
12 Y. Chen, P. Li, P. H. Huang, Y. Xie, J. D. Mai, L. Wang, N. T. Nguyen and T. J. Huang, *Lab Chip*, 2014, **14**, 626–645.
13 M. Kapałczyńska, T. Kolenda, W. Przybyła, M. Zajączkowska, A. Teresiak, V. Filas, M. Ibbs, R. Bliźniak, Ł. Łuczewski and K. Lamperska, *Arch. Med. Sci.*, 2018, **14**, 910–919.
14 H. Page, P. Flood and E. G. Reynaud, *Cell Tissue Res.*, 2013, **352**, 123–131.
15 N. Gupta, J. R. Liu, B. Patel, D. E. Solomon, B. Vaidya and V. Gupta, *Bioeng. Transl. Med.*, 2016, **1**, 63–81.
16 N. M. Anderson and M. C. Simon, *Curr. Biol.*, 2020, **30**, R921–R925.
17 X. Lei, Y. Lei, J. K. Li, W. X. Du, R. G. Li, J. Yang, J. Li, F. Li and H. B. Tan, *Cancer Lett.*, 2020, **470**, 126–133.
18 X. Xiang, J. Wang, D. Lu and X. Xu, *Signal Transduction Targeted Ther.*, 2021, **6**, 75.
19 M. J. Pittet, O. Michielin and D. Migliorini, *Nat. Rev. Clin. Oncol.*, 2022, **19**, 402–421.
20 K. Białkowska, P. Komorowski, M. Bryszewska and K. Miłowska, *Int. J. Mol. Sci.*, 2020, **21**, 1–17.
21 A. Tevlek, S. Kecili, O. S. Ozcelik, H. Kulah and H. C. Tekin, *ACS Omega*, 2023, **8**, 3630–3649.
22 J. Ro, J. Kim and Y. K. Cho, *Analyst*, 2022, **147**, 2023.
23 K. Moshksayan, N. Kashaninejad, M. E. Warkiani, J. G. Lock, H. Moghadas, B. Firoozabadi, M. S. Saidi and N. T. Nguyen, *Sens. Actuators, B*, 2018, **263**, 151–176.
24 Y. Wang, M. Liu, Y. Zhang, H. Liu and L. Han, *Lab Chip*, 2023, **23**, 1080–1096.
25 C. Parent, K. Raj Melayil, Y. Zhou, V. Aubert, D. Surdez, O. Delattre, C. Wilhelm and J.-L. Viovy, *Lab Chip*, 2023, **23**, 5139–5150.
26 J. M. Lee, J. W. Choi, C. D. Ahrberg, H. W. Choi, J. H. Ha, S. G. Mun, S. J. Mo and B. G. Chung, *Microsyst. Nanoeng.*, 2020, **6**, 52.
27 L. Yu, M. C. W. Chen and K. C. Cheung, *Lab Chip*, 2010, **10**, 2424–2432.
28 D. Rodoplu, J. S. Matahum and C. H. Hsu, *Lab Chip*, 2022, **22**, 1275–1285.
29 O. Frey, P. M. Misun, D. A. Fluri, J. G. Hengstler and A. Hierlemann, *Nat. Commun.*, 2014, **5**, 4250.
30 A. Y. Hsiao, Y. S. Torisawa, Y. C. Tung, S. Sud, R. S. Taichman, K. J. Pienta and S. Takayama, *Biomaterials*, 2009, **30**, 3020–3027.
31 K. Kwapiszewska, A. Michalczuk, M. Rybka, R. Kwapiszewski and Z. Brzózka, *Lab Chip*, 2014, **14**, 2096–2104.
32 B. Patra, Y. H. Chen, C. C. Peng, S. C. Lin, C. H. Lee and Y. C. Tung, *Biomicrofluidics*, 2013, **7**, 054114.
33 T. Mulholland, M. McAllister, S. Patek, D. Flint, M. Underwood, A. Sim, J. Edwards and M. Zagnoni, *Sci. Rep.*, 2018, **8**, 14672.
34 S. Kheiri, Z. Chen, I. Yakavets, F. Rakhshani, E. W. K. Young and E. Kumacheva, *Biotechnol. J.*, 2023, **18**, 2200621.
35 S. Kheiri, I. Yakavets, J. Cruickshank, F. Ahmadi, H. K. Berman, D. W. Cescon, E. W. K. Young and E. Kumacheva, *Adv. Mater.*, 2024, **36**, 2410547.
36 M. C. Kim, Z. Wang, R. H. W. Lam and T. Thorsen, *J. Appl. Phys.*, 2008, **103**, 044701.
37 L. Y. Wu, D. Di Carlo and L. P. Lee, *Biomed. Microdevices*, 2008, **10**, 197–202.
38 W. Liu, J. C. Wang and J. Wang, *Lab Chip*, 2015, **15**, 1195–1204.
39 C. Y. Fu, S. Y. Tseng, S. M. Yang, L. Hsu, C. H. Liu and H. Y. Chang, *Biofabrication*, 2014, **6**, 015009.
40 S. J. Hao, Y. Wan, Y. Q. Xia, X. Zou and S. Y. Zheng, *Adv. Drug Delivery Rev.*, 2018, **125**, 3–20.
41 H. Chen, Z. Zhang and B. Wang, *AIP Adv.*, 2018, **8**, 120701.
42 K. W. Oh, K. Lee, B. Ahn and E. P. Furlani, *Lab Chip*, 2012, **12**, 515–545.
43 M. J. Mitchell and M. R. King, *New J. Phys.*, 2013, **15**, 015008.
44 R. Fan, T. Emery, Y. Zhang, Y. Xia, J. Sun and J. Wan, *Sci. Rep.*, 2016, **6**, 27073.
45 A. Marrella, A. Fedi, G. Varani, I. Vaccari, M. Fato, G. Firpo, P. Guida, N. Aceto and S. Scaglione, *PLoS One*, 2021, **16**, e0245536.
46 S. Dasari and P. B. Tchounwou, *Eur. J. Pharmacol.*, 2014, **740**, 364–378.
47 X. Yan, F. L. Liang, D. Li and J. Zheng, *Mol. Cell. Biochem.*, 2015, **398**, 95–104.
48 C. Mayr, T. Kiesslich, D. Bekric, M. Beyreis, M. Kittl, C. Ablinger, E. Neureiter, M. Pichler, F. Prinz, M. Ritter, D. Neureiter, M. Jakab and H. Dobias, *PLoS One*, 2023, **18**, e0287769.
49 S. Gkountela, F. Castro-Giner, B. M. Szczerba, M. Vetter, J. Landin, R. Scherrer, I. Krol, M. C. Scheidmann, C. Beisel, C. U. Stirnimann, C. Kurzeder, V. Heinzelmann-Schwarz, C. Rochlitz, W. P. Weber and N. Aceto, *Cell*, 2019, **176**, 98–112.e14.
50 S. Comsa, A. M. Cimpean and M. Raica, *Anticancer Res.*, 2015, **35**, 3147–3154.
51 A. Dittmer, K. Hohlfeld, J. Lützkendorf, L. P. Müller and J. Dittmer, *Cell. Mol. Life Sci.*, 2009, **66**, 3053–3065.
52 H. E. Amirabadi, M. Tuerlings, A. Hollestelle, S. SahebAli, R. Luttge, C. C. van Donkelaar, J. W. M. Martens and J. M. J. den Toonder, *Biomed. Microdevices*, 2019, **21**, 101.
53 C. L. Dietsche, E. Hirth and P. S. Dittrich, *Lab Chip*, 2022, **23**, 362–371.
54 Y. Pan, Y. Yu, X. Wang and T. Zhang, *Front. Immunol.*, 2020, **11**, 583084.
55 A. Mantovani, F. Marchesi, A. Malesci, L. Laghi and P. Allavena, *Nat. Rev. Clin. Oncol.*, 2017, **14**, 399–416.
56 C. Kerneur, C. E. Cano and D. Olive, *Front. Immunol.*, 2022, **13**, 1026954.
57 P. Chauhan, A. Sodhi and A. Shrivastava, *Immunobiology*, 2009, **214**, 197–209.

58 I. Larionova, N. Cherdyntseva, T. Liu, M. Patysheva, M. Rakina and J. Kzhyshkowska, *OncoImmunology*, 2019, **8**, e1596004.
59 A. Mantovani and P. Allavena, *J. Exp. Med.*, 2015, **212**, 435–445.
60 P. Zheng, L. Chen, X. Yuan, Q. Luo, Y. Liu, G. Xie, Y. Ma and L. Shen, *J. Exp. Clin. Cancer Res.*, 2017, **36**, 36–53.
61 X. Xu, S. Xu, L. Jin and E. Song, *Pattern Recognit. Lett.*, 2011, **32**, 956–961.